www.czasopisma.pan.pl PAN POLSKA AKADEMIA NAUK www.journals.pan.pl

Arch. Metall. Mater. **67** (2022), 4, 1315-1324

DOI: https://doi.org/10.24425/amm.2022.141057

QIHANG PANG[1,2], CONG GENG[1,2], JIAJI WANG[2*], WEIJUAN LI[1,2], JING GUO[1,2], XIAOMING YU[3]

INTERNAL FRICTION STUDY ON THE INFLUENCE OF PRE-DEFORMATION ON HYDROGEN EMBRITTLEMENT SENSITIVITY OF DUAL-PHASE STEEL

In this study, an electrochemical method was used to permeate hydrogen through annealed DP590 steel under various pre-strain conditions (0-15%). Stress-strain and internal friction-temperature curves of the dual phase (DP) steel were obtained from slow strain-rate tensile tests and internal friction measurements, respectively. The diffusion of interstitial atoms, formation of Cottrell atmospheres, and embrittlement mechanism of DP steel were investigated under different prestress conditions before and after hydrogen permeation. The results show that the tensile strength of DP steel first decreases and then increases and the elongation sharply decreases with increasing pre-strain. The strength and ductility present similar trends with changes in pre-strain before and after hydrogen charging, however, after hydrogen charging, an obvious increase in tensile strength and decrease in elongation are observed. Furthermore, the γ peak amplitude decreases and the Snoek-Ke-Koster (SKK) peak amplitude increases with increasing internal pre-strain according to the friction-temperature curve. The γ peak and SKK peak exhibit the same trends with increasing pre-strain before and after hydrogen charging and both the γ peak and SKK peak decrease with hydrogen charging. The dislocation density in DP steel increases after hydrogen charging.

Keywords: Dual phase steel; hydrogen embrittlement; γ peak; SKK peak; dislocation density

1. Introduction

Dual phase (DP) steels are widely used in side beams, chassis reinforcements, and structural components of automobiles owing to their low flexural strength ratio and high tensile elongation [1]. However, not all the hydrogen generated during the fabrication process of DP steel is eliminated, which with PPm level can lead to hydrogen embrittlement, and ultimately, brittle fracture under the stress [2]. Chen, et al. [3] found that the hydrogen embrittlement sensitivity of dual-phase steel (F+M) has a peak value with the increase of cold drawing deformation. The microstructure shows that the micro-crack will gather and grow at the hydrogen carrying dislocation first, and finally fracture. Therefore, research on the hydrogen embrittlement sensitivity of DP steel is critical to ensuring the safety of automobile parts and structures.

Currently, hydrogen embrittlement is mainly studied using electrochemical hydrogen permeation methods. Depover [4] investigated the hydrogen embrittlement sensitivity of DP steel (F+M) and found that strength of the steel first decreases and then increases with increasing current density at low tensile strain rates. At higher tensile strain rates, the strength first increases and then decreases and elongation gradually decreases with increasing current density. The yield strength and elongation of multiple phase 780 MPa transformation-induced plasticity (TRIP) steel were both found to decrease with increasing hydrogen permeation time and hydrogen embrittlement sensitivity continuously increases [5]. Ronevich [6] studied the variation of mechanical properties of several high-strength steels (DP600: Dual phase steel with tensile strength of 600MPa; TRIP780: TRIP steel with tensile strength of 780MPa, TRIP980: TRIP steel with tensile strength of 980MPa, and M220: martensite steel) with hydrogen content and showed that an increase in hydrogen content leads to a decrease in elasticity, M220 > TRIP780 > TRIP980 > DP600. Notably, the tensile strength of TRIP980 first increased and then decreased with increasing hydrogen content, whereas the tensile strength of the other steels continued to decrease. Among them, the strength of M220 changed dramatically after hydrogen permeation and fractured during the elastic deformation stage, exhibiting a complete loss in ductility.

[1] UNIVERSITY OF SCIENCE AND TECHNOLOGY LIAONING, SCHOOL OF MATERIALS AND METALLURGY, ANSHAN LIAONING, 114051, CHINA
[2] STATE KEY LABORATORY OF METAL MATERIAL FOR MARINE EQUIPMENT AND APPLICATION, ANSHAN LIAONING, 114009, CHINA
[3] SHENYANG LIGONG UNIVERSITY, SCHOOL OF MATERIAL SCIENCE AND ENGINEERING, SHENYANG LIAONING, 110159, CHINA

* Corresponding author: 280100886@qq.com

Hydrogen has a small atomic radius and diffuses easily in steel, therefore, conventional methods for detecting and characterizing gases cannot accurately detect or characterize hydrogen. The internal friction peak can be used to characterize dislocations and grain boundary movements in metals. Hydrogen interacts with dislocations and grain boundaries as it enters the metal matrix, which changes the internal friction peak. At present, hydrogen-induced internal friction peaks can be divided into three types: peaks above 200°C, internal friction relaxation peaks, and Snoek peaks. Ge [7] and Cantelli [8] discovered hydrogen-induced internal friction peaks near 275°C (38CrMoAl steel) and 230°C (pure Ni), respectively, following hydrogen permeation via electrolysis. The internal friction relaxation peak is caused by interactions between hydrogen and grain boundaries. Zhang [9] observed a hydrogen-induced internal friction peak in Fe-Ni-Cr alloy (between 26-36°C) after charging the austenitic alloy with hydrogen from the hot gas phase. The peak was considered an internal friction relaxation peak generated by interactions between hydrogen and grain boundaries containing a small amount of carbide. Finally, the Snoek peak of hydrogen is observed at low temperatures and is generally attributed to the interaction of dislocations with hydrogen [10-12].

In DP steel, stress concentrations as well as many crystal defects at grain boundaries are generated during the plastic deformation process. Crystal defects act as traps to absorb hydrogen, thereby increasing the hydrogen embrittlement sensitivity of the steel. In this study, the internal friction method was used to investigate the hydrogen embrittlement sensitivity of DP steel and the influence of hydrogen charging on the internal friction peak under different pre-strain conditions. Furthermore, the hydrogen-induced fracture mechanism in DP steel was revealed.

2. Experimental

The chemical composition of the annealed DP steel used in the experiment is listed in TABLE 1, and its chemical composition was measured according to the national standards of GB/T20066-2006. The DP steel was mainly composed of fine polygonal ferrite with an average grain size of 13.7 μm and small islands of martensite, as shown in Fig. 1. Flat-plate samples with dimensions of 50 mm×10 mm×1.5 mm were polished and ultrasonically cleaned prior to hydrogen permeation. The electrochemical hydrogen permeation tests involved a single electrolytic cell structure, as shown in Fig. 2. The electrolytic solution contained 0.2 mol/L NaOH solution and 2 mL saturated Na_2S solution as a toxicant to prevent the formation and release of H_2 molecules [13]. The applied current density was 10 mA/cm^2. Hydrogen permeability measurements were performed using the Devanathan-Nishimura method [14].

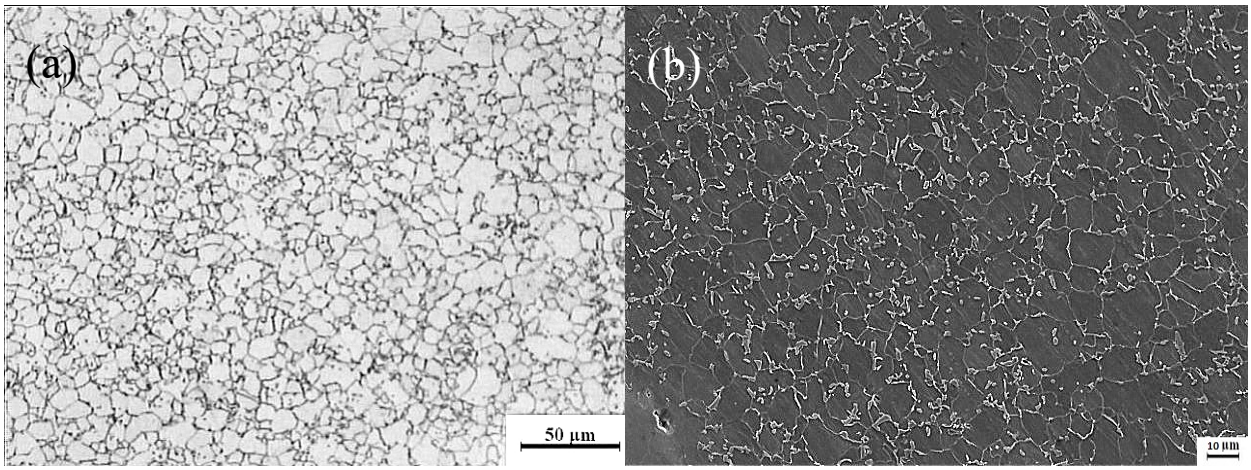

Fig. 1. Microstructure of annealed DP steel: (a) Optical microscopy, (b) Scanning electron microscopy

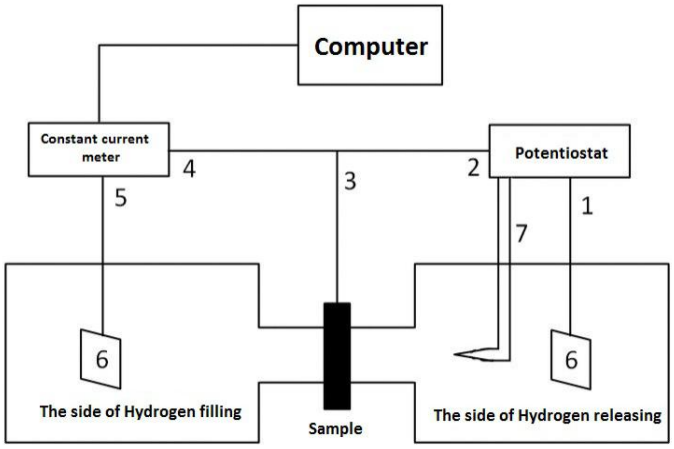

Fig. 2. Schematic illustration of hydrogen permeation experiment 1) Auxiliary electrode terminal; 2) Reference electrode terminal; 3) Working electrode; 4) Cathode terminal of current meter; 5) Anode terminal column of constant current meter; 6) Platinum electrode; 7) Reference electrode

TABLE 1

Chemical composition of annealed DP steel (wt.%)

C	Si	Mn	P	S	Al
0.068	0.25	1.35	0.013	0.006	0.038

Internal friction measurements were performed using the method of natural oscillation (amplitude of 30) with an MFP-1000 multi-functional internal friction instrument. Specimens with dimensions of 1 mm × 2.4 mm × 50 mm were tested in the temperature range of –120-300°C at a heating rate of about 3°C /min. Tensile tests were carried out on a MFDL100 slow strain rate tensile testing machine at a strain rate of 0.003 mm/min. The sample dimensions are shown in Fig. 3. The standard distance section of the sample was completely immersed in a tank filled with electrolytic hydrogen. The test was stopped when the sample fractured and the fracture morphology was subsequently observed by the LEO-1450 scanning electron microscopy (SEM).

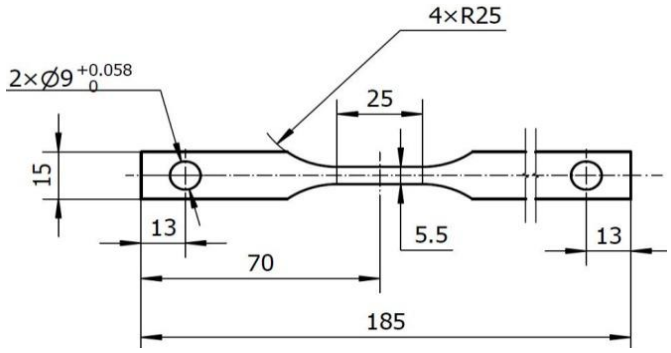

Fig. 3. Dimensions of specimens used in slow strain rate tensile tests / mm

3. Results

3.1. Diffusion behavior of hydrogen in DP steel

The hydrogen permeability of DP steel is shown in Fig. 4. The hydrogen diffusivity rate D can be calculated as [15]

$$D = \frac{L^2}{6t_{0.63}} \tag{1}$$

where D is the hydrogen diffusion rate (cm^2/s), L is the sample thickness (cm), $t_{0.63}$ is the time corresponding to $0.63I_\infty$ (s), and I_∞ is the steady-state current (μA).

Assuming a semi-infinite medium and constant diffusion, the maximum distance that hydrogen atoms can diffuse in time T is

$$X_{max} = 4\sqrt{Dt} \tag{2}$$

According to equation (1), the hydrogen diffusivity rate D was 0.806×10^{-6} cm^2/s and according to equation (2) [15], the time t required for hydrogen to diffuse from one end to the other was 233 min. The hydrogen filling time was set to 300 min, which is larger than the theoretical value, and the current density was 10 mA/cm^2; Therefore, the hydrogen could effectively penetrate the sample. The hydrogen content of samples (50 mm × 10 mm × 1.5 mm) was estimated by the American company RH-600 Hydrogen determinator, and the measurement error is ≤±5%. TABLE 2 presents the change in hydrogen content in DP steel before and after hydrogen permeation, which is similar to previously published data [16]. The hydrogen content in the DP steel increased from 1.24 ppm to 2.08 ppm.

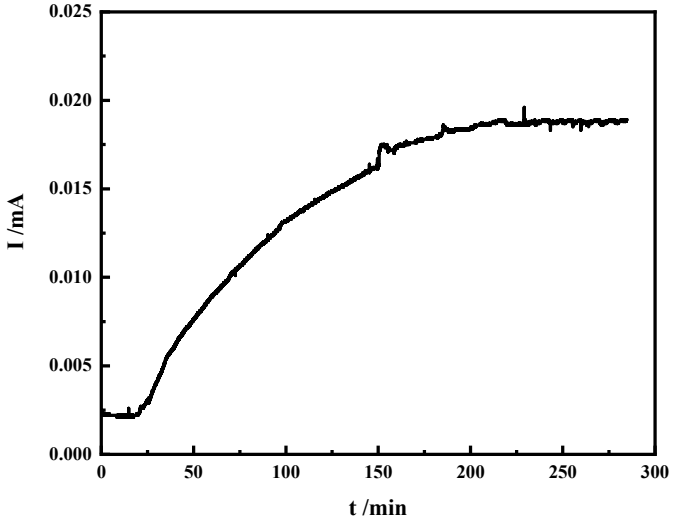

Fig. 4. Hydrogen permeability of DP steel

TABLE 2

Hydrogen content in DP steel (ppm)

	1st	2nd	Average value
$C_{H\text{-}before}$	0.920±0.046	1.551±0.077	1.243±0.062
$C_{H\text{-}after}$	1.784±0.089	2.373±0.118	2.082±0.104

The dislocation structure was investigated in a JEM-2100 transmission electron microscope (TEM). TEM specimens of 50 μm thickness were prepared by mechanical grinding and electro-polishing with a twin jet electro-polisher at –20°C using a solution containing 80 vol.-% C_2H_5OH and 20 vol.-% $HClO_4$. Fig. 5 shows the dislocation morphology in DP steel without deformation before and after hydrogen charging. Previous studies have shown that defects in steel, such as vacancies, grain boundaries, and dislocations, can trap hydrogen atoms, thereby hindering hydrogen diffusion [17]. However, the diffusion of hydrogen also had a certain influence on the dislocation morphology (Fig. 5). The length of the dislocation line and dislocation density significantly increased after hydrogen charging, indicating that hydrogen permeation can increase the dislocation density without deformation.

During the initial stage of hydrogen diffusion, due to the migration of interstitial hydrogen atoms, many vacancies are present as dislocation sources, which promotes the generation and movement of dislocations. Hydrogen increases the dislocation density and induces local softening or hardening, which is related to the density of movable and immovable dislocations. When the proportion of immovable dislocations increases, hardening is more evident. Without deformation, the “hydrogen mass” moves with the dislocation movement. Dislocations act as a hydrogen traps until grain boundaries or other obstacles appear, resulting in dislocation accumulation.

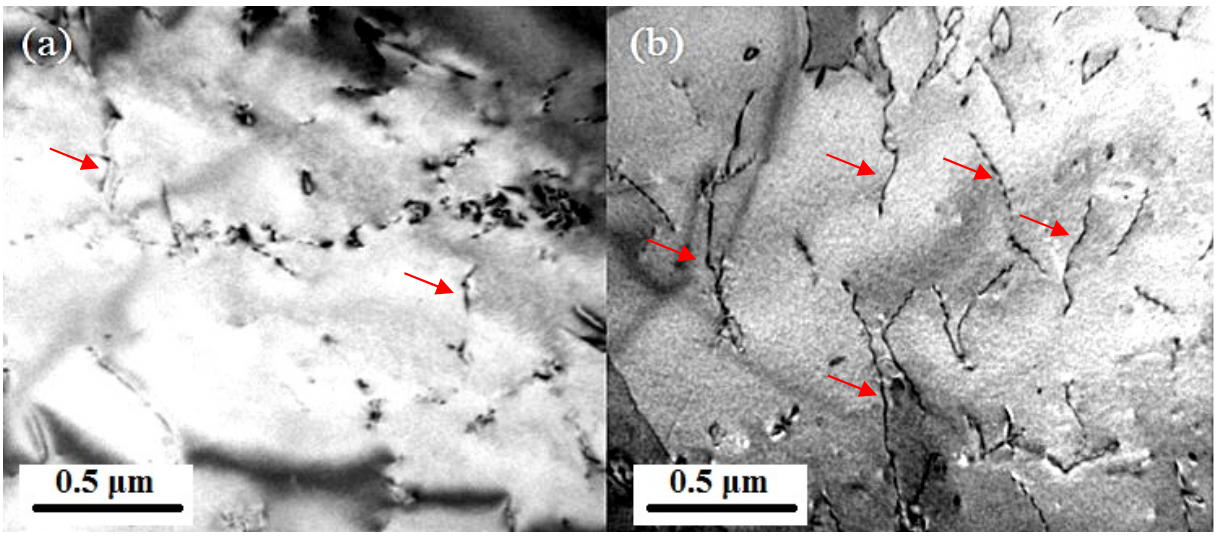

Fig. 5. Dislocation morphology in DP steel specimens: (a) H-uncharged, (b) H-charged

3.2. Effect of hydrogen charging on mechanical properties

Fig. 6 shows stress-strain curves before and after hydrogen charging under different pre-strain conditions. The elastic deformation was small and the strength of the steel increased due to work hardening generated by rapid plastic deformation. For non-hydrogen-permeated samples, the tensile strength was reached at the end of the uniform plastic deformation stage and final fracture occurred during non-uniform deformation, i.e., during necking.

With increasing pre-strain, the tensile strength firstly decreased then increased, whereas the elongation gradually decreased. During the pre-strain process, the tensile strength increased, however, the elongation decreased obviously. A Cottrell atmosphere was formed and the movement of hydrogen matched the dislocation motion at low strain rates and certain temperatures. In other words, the Cottrell atmosphere moves with, and eventually lags behind, dislocation movements and plays a role in dislocation pinning, leading to local work hardening.

Plastic deformation was caused by movement of dislocations, which were also covered by hydrogen atoms and formed new hydrogen clumps. When the dislocations and hydrogen mass move under the action of external forces, dislocation accumulation will occur near grain boundaries or other obstacles and hydrogen accumulation will also inevitably occur near grain boundaries. If the stress is large enough, stress concentrations will lead to crack formation at the ends of accumulated dislocations. Due to the presence of hydrogen atoms, cracks will easily form and expand, eventually leading to brittle fracture.

Fig. 7 shows the fracture morphologies at a slow strain rate before and after hydrogen charging with 0% and 15% pre-strain. Without pre-strain, dimples are uniformly distributed, whereas 15% pre-strain resulted in large dimples and ductile fracture of the non-hydrogen-charged samples. After hydrogen charging, the fracture appeared flat and bright. Although necking was

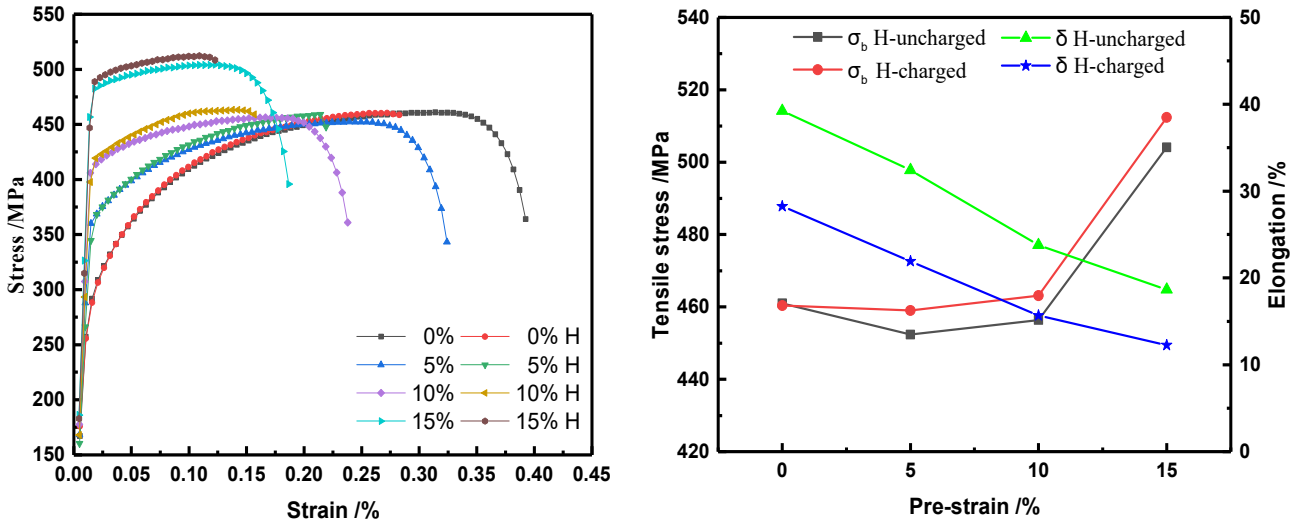

Fig. 6. Tensile properties of DP steel under different pre-strain conditions: (a) Stress-strain curves after hydrogen charging, (b) Elongation and tensile strength

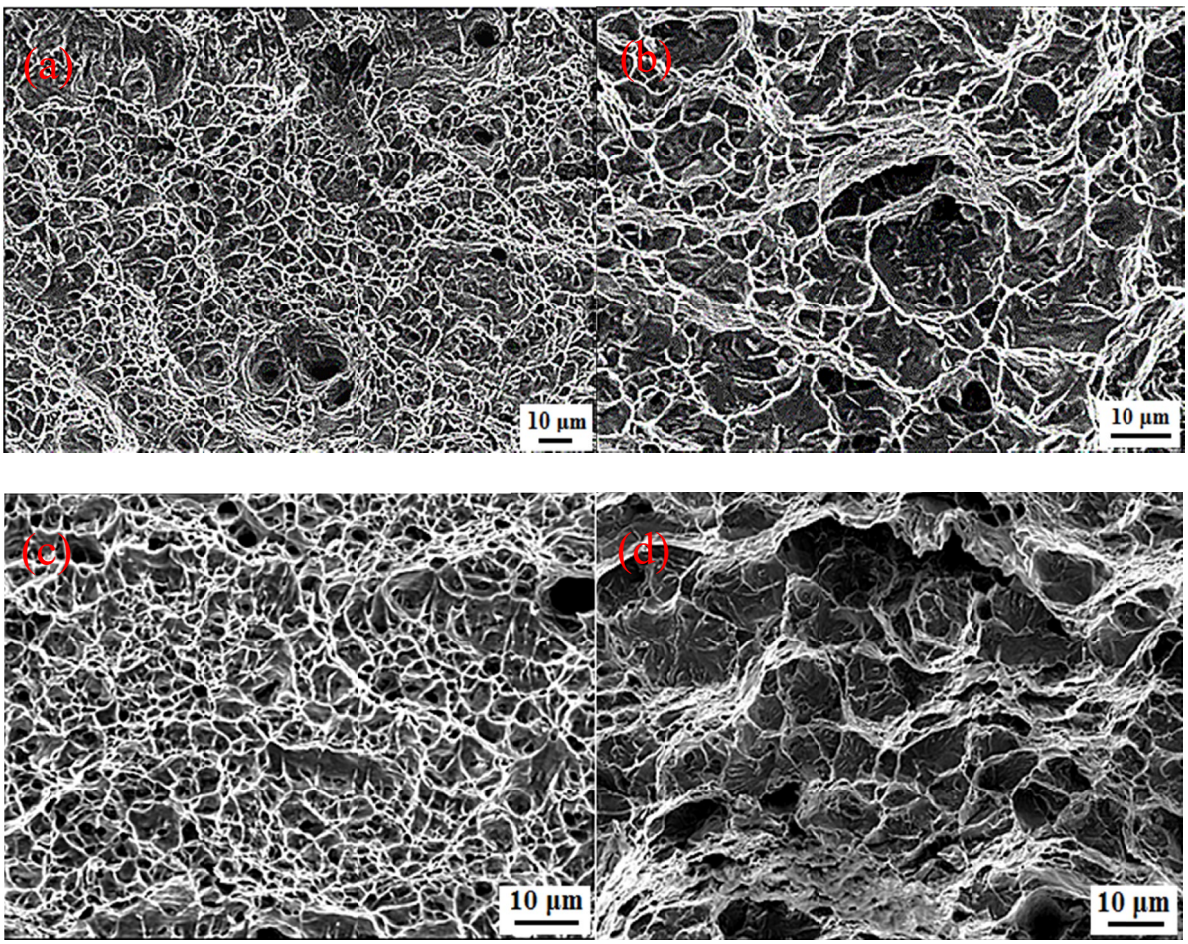

Fig. 7. Tensile fracture morphology of DP steel before and after H charging with different pre-strain conditions: (a) 0%, H-uncharged, (b) 0%, H-charged, (c) 15%, H-uncharged, (d) 15%, H-charged

not observed, an area of obvious plastic deformation can be observed. Small dimples appeared with 5% pre-strain, indicating ductile fracture. When the pre-strain was increased to 15%, the number of river-like cleavage planes dramatically increased, as shown in Fig. 7(d), and the fracture mode changed from ductile to brittle fracture.

With the increase in pre-strain, the number of defects, such as dislocations, increased and the entanglement and capture of hydrogen atoms also increased, which intensifies the hydrogen atom enrichment. Hydrogen atoms above the "critical concentration" not only promote the initiation of microcracks at the ends of dislocation accumulations but can also cause crack propagation due to local "hydrogen pressure", which induces brittle fracture.

3.3. Internal friction experiment

Fig. 8(a-h) shows the internal friction-temperature curves of the steel before and after hydrogen charging under different pre-strain conditions. Three obvious internal friction peaks can be observed at 39ºC, 70ºC, and 200ºC. The peaks are denoted P_{D1}, P_{D2}, P_{D3}, according to temperature (from low to high). With increasing pre-strain, P_{D1} tends to move slightly towards lower temperatures, whereas no obvious changes in P_{D2} and P_{D3} can be observed. TABLE 3 summarizes the P_{D1}, P_{D2}, and P_{D3} data. The activation energy of the internal friction peak can be calculated as [18]

$$H = RT_m \ln \frac{K_B T_m}{h f_m / N_A} + T_m \Delta S \tag{3}$$

where R = 8.3144 $JK^{-1}mol^{-1}$, K_B = 1.380658×10^{-23} $J\cdot K^{-1}$, h = 6.6260755×10^{-34} J·S, ΔS = 1.1×10^{-4} $Ev\cdot K^{-1}$, 1eV = 1.602×10^{-19} J, and N_A = 6.02×10^{23} mol^{-1}. The activation energy was 0.79 eV, 0.88 eV, and 1.20 eV for the P_{D1}, P_{D2}, P_{D3} peaks, respectively. Similar to previous reports [19-22], P_{D1} can be considered the γ peak, P_{D2} is the Snoek peak, and P_{D3} is the SKK peak.

4. Discussion

4.1. Influence of pre-strain on internal friction

Fig. 9 shows the changes in three internal friction peaks of DP steel with increasing pre-strain before and after hydrogen charging. The internal friction diagram shows no internal friction peak at low temperature. Therefore, the hydrogen content was

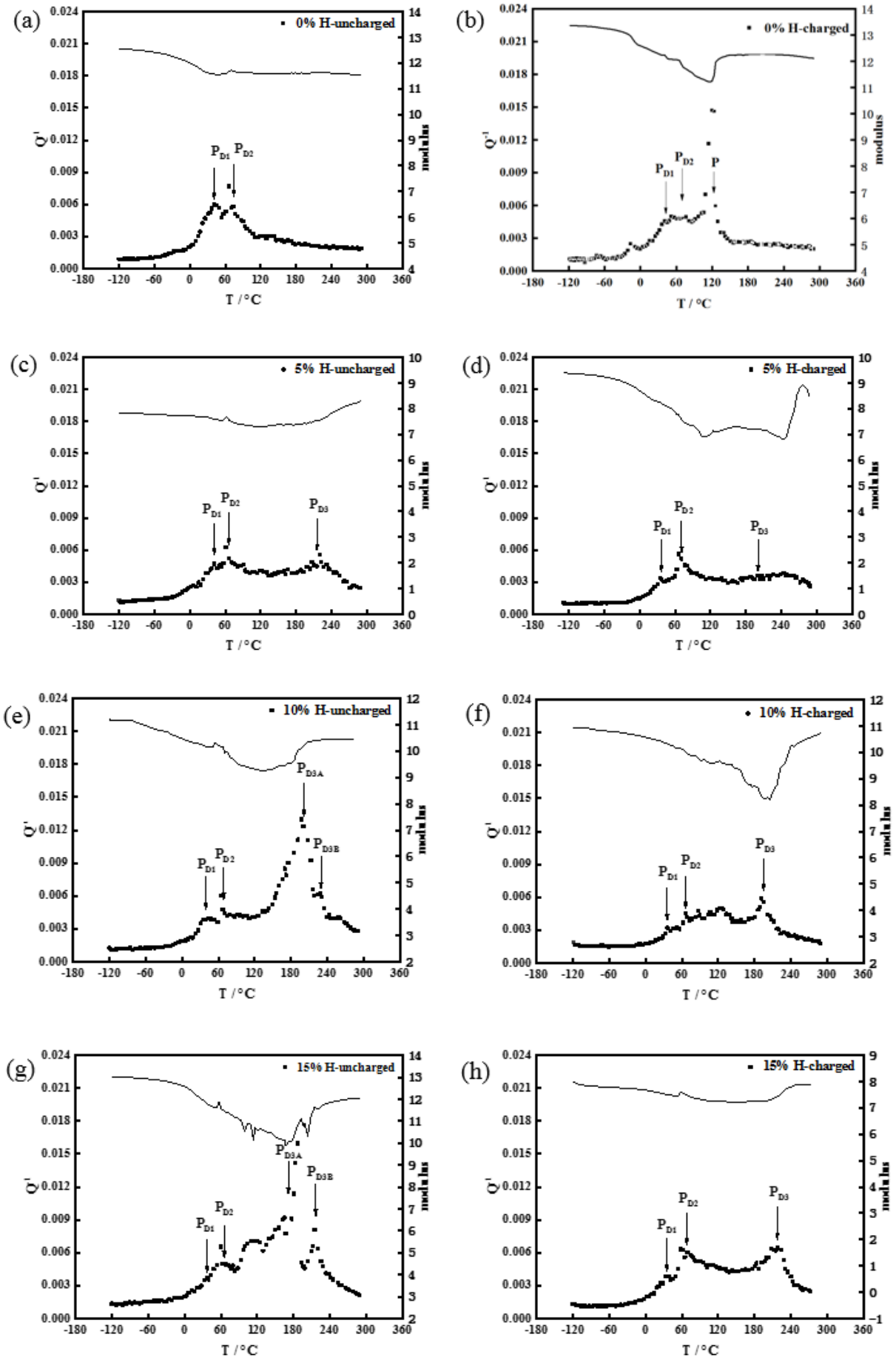

Fig. 8. Internal friction curve of DP steel before and after hydrogen charging under different pre-strain conditions: (a) 0%, H-uncharged; (b) 0%, H-charged; (c) 5%, H-uncharged; (d) 5%, H-charged; (e) 10%, H-uncharged; (f) 10%, H-charged; (g) 15%, H-uncharged; (h) 15%, H-charged

TABLE 3

Internal peak temperature, frequency, activation energy, and internal friction value of DP steel with or without H charging under different pre-strain conditions

	Samples	T_m (°C)	F_m (Hz)	H (eV)	Q^{-1}
P_{D1}	0% H-uncharged	41.1	3.403	0.80052	0.00592
	0% H-charged	41	3.498	0.79951	0.00437
	5% H-uncharged	41.5	2.757	0.80728	0.00433
	5% H-charged	37.7	3.286	0.79250	0.00314
	10% H-uncharged	38.4	3.192	0.79512	0.0039
	10% H-charged	36	3.208	0.78865	0.00291
	15% H-uncharged	36.4	3.436	0.78788	0.00389
	15% H-charged	37.8	2.74	0.79763	0.00362
P_{D2}	0% H-uncharged	73.4	3.418	0.88563	0.00566
	0% H-charged	72	3.431	0.88182	0.00481
	5% H-uncharged	66.1	2.75	0.87270	0.00491
	5% H-charged	70.7	3.315	0.87940	0.00499
	10% H-uncharged	67.3	3.029	0.87306	0.00475
	10% H-charged	72.5	3.191	0.88530	0.00482
	15% H-uncharged	67.7	3.378	0.87091	0.00476
	15% H-charged	69.5	2.734	0.88192	0.00597
P_{D3}	0% H-uncharged	—	—	—	—
	0% H-charged	—	—	—	—
	5% H-uncharged	215.2	2.747	1.27180	0.00469
	5% H-charged	199.9	3.235	1.22398	0.00342
	10% A H-uncharged	191.6	3.103	1.20346	0.00533
	10% B H-uncharged	228.5	3.304	1.29963	0.0062
	10% H-charged	191.4	2.727	1.20809	0.00865
	15%A H-uncharged	171.4	3.171	1.14860	0.0087
	15%B H-uncharged	212.1	3.377	1.25483	0.00597
	15% H-charged	214.9	2.723	1.27136	0.00642

assumed to be low at the interstitial void of DP steel, which was not the main location of hydrogen diffusion.

As shown in Fig. 9(a), the γ peak of body-centered cubic (*bcc*) metals is equivalent to Bordoni relaxation in face-centered cubic (*fcc*) metals [17]. γ relaxation is associated with the diffusion of kinks on $a/2<111>$ screw dislocations along {110} or {112} glide planes [23]. Moreover, Jung [14] found that the γ peak amplitude depends on dislocation density and dislocation segment length. According to Seeger [24], the relationship between relaxation intensity, i.e., internal friction, and dislocation density can be expressed as

$$\Delta = \frac{8\eta L^2 a^2 b^2 M}{\pi^4 kT}\rho_d \tag{4}$$

Where a represents the distance between the adjacent Peierls valley; L is the non-relaxation elastic modulus; ρ_d is the dislocation density, assuming all sections contain η geometric knots and L potential wells; Δ denotes the relaxation strength; $M = (L\cos\varphi)/b$, b is the period of the kink potential along the close-packed direction, and φ denotes the angle between the average direction of the dislocation and the close-packed direction. Equation (4) shows that relaxation intensity is proportional to dislocation density. The peak value, i.e., relaxation intensity, decreases with increasing pre-strain. As the amount of pre-strain increases, the number of knots on $a/2<111>$ screw dislocations along {110} or {112} glide surfaces in the DP steel decrease. Normally, dislocation density tends to increase with increasing pre-strain, however, too many dislocations can become entangled with each other, which restricts dislocation movement. Thus, the number of screw dislocations diffusing along a particular glide plane will decrease and γ relaxation intensity will decrease.

The γ peak amplitude decreased after hydrogen charging. Hydrogen can promote dislocation motion, however, for cross slip of a mixed dislocation to occur, it must turn into a full-screw dislocation. After hydrogen charging, the energy of the transition from edge dislocation to screw dislocation increased; that is, hydrogen filling hinders the transition [13]; Therefore, under the same pre-deformation without external tensile stress, the number of dislocations in the DP steel was stable. After hydrogen charging, it was difficult for edge dislocations to transform into screw dislocations; Whereas, hydrogen filling promoted dislocation slip of the whole screw type. The dislocation moved to the grain boundary and the phase boundary cancelled with each other, which led to a decrease in the number of screw dislocations moving along a particular slip plane in the DP steel.

Fig. 9(b) shows the changes of peak value in the Snoek peak with pre-strain and hydrogen charging. Snoek peak refers to the internal friction peak near 40°C on the vibration attenuation-tem-

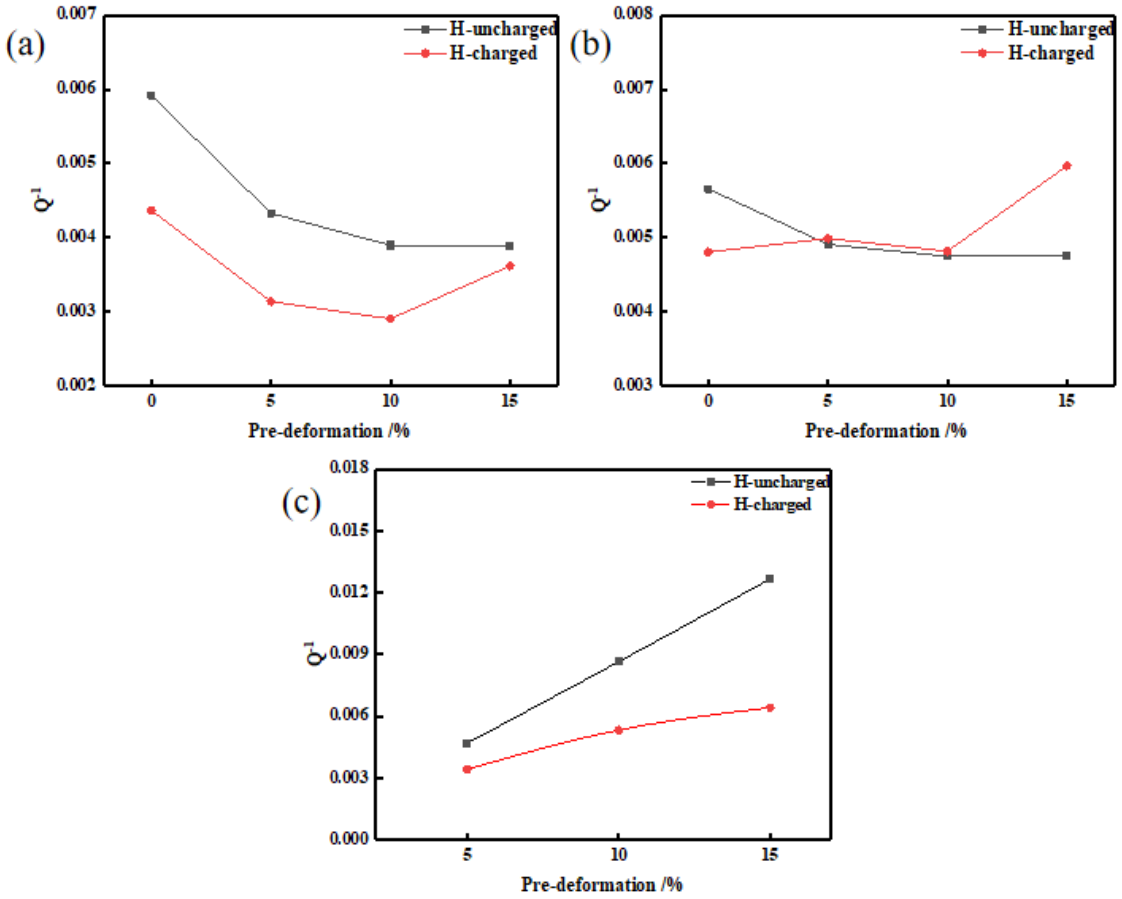

Fig. 9. Internal friction peaks before and after hydrogen charging of DP steel with different pre-strain conditions: (a) γ peak, (b) Snoek peak, (c) SKK peak

perature curve of carbon steel. This peak is in direct proportion to the content of carbon (or nitrogen) atoms, and its activation energy is exactly equal to the activation energy of carbon (or nitrogen) atoms diffusion in iron. Therefore, it is believed that this peak is caused by the micro diffusion of carbon atoms in iron. Without hydrogen charging, the peak amplitude decreased and gradually stabilized as the pre-strain was increased. The Snoek peak amplitude represents the interstitial carbon content. Based on the changes in internal friction peak, the interstitial carbon content remained relatively stable with a pre-strain of 5-10%, and slightly increased after hydrogen charging. The opposite trend was observed for interspace carbon atom content with a pre-strain of 10-15%. It is because after hydrogen charging, the equilibrium of solute atom ordering realized by the micro-diffusion of interstitial atoms such as carbon (or nitrogen) atom is broken, and a new dynamic equilibrium is formed between hydrogen atom, hydrogen trap and carbon (or nitrogen) atom.

Fig. 9(c) shows the variation of SKK peak amplitude with pre-strain before and after hydrogen charging. The SKK peak is the internal friction peak caused by the Cottrell atmosphere dragged by non-screw dislocations in the bcc material. The internal friction diagram indicates that the SKK peak did not appear with no pre-strain as shown in Fig. 8a. After hydrogen charging, although the peak appeared at 120°C, the number of points was small, and it is not the temperature range that the SKK peak usually occurs in (such as the literature[19-22]). Therefore, the peak is not the SKK peak after hydrogen charging, as shown in Fig. 8b. In Fig. 8c, the SKK peak appeared at about 200ºC with a pre-strain of 5%. Owing to the wide and low SKK peak under H-charged, the temperature cannot be easily confirmed. When the pre-strain was 10%, the SKK peak was decomposed into two peaks at 190ºC and 218ºC. The peak amplitude increased, and the entire peak became sharper. A possible reason for peak splitting is that the strength of non-screw dislocation pinning by interstitial atoms are different in bcc ferrite and bcc martensite, therefore, the energy required for non-screw dislocation movement will be different. After hydrogen charging, only one SKK peak appeared and the peak amplitude decreases slightly. When the pre-strain was 15%, the SKK peak was also decomposed into two peaks, and only one SKK peak appeared after hydrogen charging.

In conclusion, when the pre-strain was increased, the peak SKK amplitude increased, indicating that the density of pinned movable non-screw dislocations in the DP steel increased. Hydrogen charging reduces the SKK peak amplitude. Moreoever, the peak SKK amplitude is mainly determined by the density of the pinned movable non-screw dislocations. Hydrogen can promote dislocation movement, therefore, pinned movable non-screw dislocation are free from this restraint and the dislocation density is reduced, causing a drop in the peak amplitude.

4.2. Influence of pre-strain on hydrogen embrittlement sensitivity of DP steel

The hydrogen embrittlement sensitivity was evaluated using the hydrogen embrittlement sensitivity index. Stress-strain curves of the samples were obtained from slow tensile tests and the relative ductility loss of the test samples before and after hydrogen filling were calculated. The hydrogen embrittlement sensitivity index can be calculated as [25]

$$HEI = \left(1 - \frac{TEL_H}{TEL_0}\right) \times 100\% \quad (5)$$

where TEL_0 and TEL_H are the total elongation of the test sample before and after hydrogen charging, respectively. The higher the *HEI* value, the greater the hydrogen embrittlement sensitivity. As shown in Figure 10, The *HEI* of DP steel tended to increase with increasing pre-strain and changed more gently above 10% pre-strain.

Pre-straining DP steel increases the number of defects such as dislocations. Dislocations act as hydrogen traps and play an important role in reversible hydrogen-induced ductility loss [26,27]. Dislocations trap diffusing hydrogen atoms and hinder their movement. Without pre-strain, the number of dislocations in DP steel is low, therefore, the number of hydrogen atoms that can be captured is small and the hydrogen embrittlement sensitivity is low.

Pre-strain increases the number of dislocations, which can form "dislocation cells" [25]. Thus, the ability to capture hydrogen is enhanced and hydrogen is more likely to accumulate around defects, such as dislocations. Besides normal diffusion, hydrogen can also be transferred to the center of the specimen through dislocation motion, such that the concentration and depth of hydrogen permeation are dramatically increased, thereby increasing the hydrogen embrittlement sensitivity. When the pre-strain is greater than 10%, the hydrogen embrittlement sensitivity of DP steel tends to be stable, which means fewer dislocations in DP steel with 10-15% pre-strain.

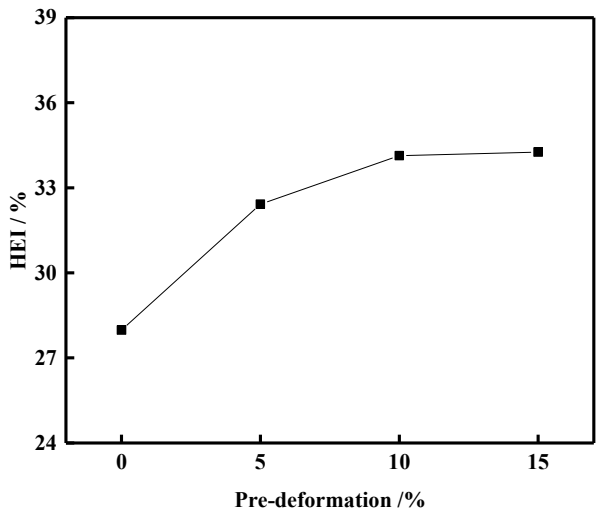

Fig. 10. Hydrogen embrittlement sensitivity index of DP steel

5. Conclusions

(1) The tensile strength of DP steel first decreased and then increased with increasing pre-strain. Hydrogen charging increased the tensile strength of DP steel and decreased the elongation. The hydrogen embrittlement sensitivity of DP steel increased with increasing pre-strain but stabilized above 10% pre-strain.

(2) With increasing pre-strain, the number of kink pairs on an $a/2<111>$ screw dislocation along the {110} or {112} slip plane decreased, causing the γ peak amplitude to decrease. After hydrogen charging, the number of screw dislocations continued to decrease and the γ peak amplitude also decreased. With increasing pre-strain, the number of non-screw dislocations increased, leading to an increase in the SKK peak amplitude. Thus, hydrogen charging promotes dislocation movement, decreases the number of pinned non-screw dislocations, and decreases the SKK peak amplitude.

Acknowledgments

This study was funded by the National Natural Science Foundation of China (Grant No. 52004122), the State Key Laboratory of Marine Equipment made of Metal Material and Application (Grant No. SKLMEA-USTL-201907), the Guidance plan of Natural Science Foundation of Liaoning Province (Grant No. 2019-ZD-0028 and 2020JH1/10100001), and the Key Projects from Liaoning Education Department (Grant No. 2019FWDF03 and 2020LNQN19).

REFERENCES

[1] C.Q. Xie, G. Wang, Y. Han, Research on hydrogen induced delayed cracking behavior of 780MPa grade dual phase steel for automotive, Hot Working Technol. **47**, 74-77 (2018).

[2] T. Depover, E. Wallaert, K. Verbeken, Fractographic analysis of the role of hydrogen diffusion on the hydrogen embrittlement susceptibility of DP steel, Mater. Sci. Eng. A **64**, 9201-208 (2016).

[3] J. Chen, C.J. Li, S.H. Zhang, Hydrogen embrittlement of cold drawn F+M dual-phase Steel, Chinese J. Eng. **12**, 339-343 (1990).

[4] T. Depover, F. Vercruysse, A. Elmahdy, P. Verleysen, K. Verbeken, Evaluation of the hydrogen embrittlement susceptibility in DP steel under static and dynamic tensile conditions, Int. J. Impact. Eng. **123**, 118-125 (2019).

[5] X.F. Yuan, Study on internal friction and mechanical properties of TRIP steel after hydrogen charging, Univ. Sci. Technol. Liaoning, 2018.

[6] J.A. Ronevich, J.G. Speer, D.K. Matlock, Hydrogen embrittlement of commercially produced advanced high strength sheet steels, Sae Int. J. Mater. Manuf. **3**, 255-267 (2010).

[7] T.S. Ge, B.C. Rong, Internal friction peak associated with the presence of hydrogen in steel, Chinese J. Phys. **10**, 153-169 (1954).

[8] R. Cantelli, F.M. Mazzolai, M. Nuovo, Internal friction due to long-range diffusion of hydrogen and deuterium in vanadium, J. Phys. Chem. Solids. **31**, 1811-1817 (1970).

[9] J. Zhang, X.Y. Li, M. Zhao, L.J. Rong, Effects of grain-boundary phases on hydrogen embrittlement of Fe-Ni-Cr austenitic alloys, Acta Metall. Sin. **44**, 1095-1098 (2008).

[10] W.J. Li, S.S. Zhao, H.Y. Zhang, Relationship between bake hardening, Snoek-Köster and dislocation-enhanced snoek peaks incoarse grained low carbon steel, Arch. Metall. Mater. **61**, 1723-1732 (2016).

[11] X.F. Yuan, W.J. Li, Q.H. Pang, Study on the performance and strain aging behavior of solid-solution state low-carbon steel, Mater. Sci. Eng. A **726**, 282-287 (2018).

[12] W.J. Li, M.Y. Cai, D. Wang, J.W. Zhang, S.S. Zhao, Studying on tempering transformation and internal friction for low carbon bainitic steel, Mater. Sci. Eng. A **679**, 410-416 (2018).

[13] W.Y. Zhu, Hydrogen Embrittlement and Stress Corrosion Cracking, Beijing: Sci. Press 2013.

[14] M. Devanathan, Z. Stachurski, W. Beck, A technique for the evaluation of hydrogen embrittlement characteristics of electroplating baths, J. Electrochem. Soc. **110**, 886- 890 (1963).

[15] X.C. Ren, W.Y. Chu, J.X. Li, L.J. Qiao, Y.J. Su, Effect of MnS inclusions on hydrogen diffusion in steel, J. Univ. Sci. Technol. Beijing **29**, 232-236 (2007).

[16] C.Q. Xie, Y. Han, S. Kuang, Research on hydrogen induced delayed cracking behavior of 590 MPa grade dual phase steel for automotive, Hot Working Technol. **46**, 104-107 (2017).

[17] I.C. Jung, D.G. Kang, B.C.D. Cooman, Impulse excitation internal friction study of dislocation and point defect interactions in ultra-low carbon bake-hardenable steel, Metall. Mater. Trans. A. **45**, 1962-1978 (2014).

[18] L.J. Baker, J.D. Parker, S.R. Daniel, The use of internal friction techniques as a quality control tool in the mild steel industry, J. Mater. Process. Technol. **143**, 442-447 (2003).

[19] H. Mizubayashi, H. Kronmüller, A. Seeger, The ν peak in deformed high-purity α-iron studied by forced vibrations out of resonance, Le J. de Phys. Coll. **46**, C10-C309 (1985).

[20] M. Shimada, K. Sakamoto. Internal friction of α-iron deformed at low temperatures, Scripta Metal. **13**, 1177-1182 (1979).

[21] S. Li, L. Deng, X. Wu, The mechanism investigation of deep cryogenic treatment on high alloy martensitic steel by low frequency internal friction, Cryogenics. **50**, 433-438 (2010).

[22] J.S. Juan, G. Fantozzi, M.L. No, C. Esnouf, Hydrogen Snoek-Koster relaxation in iron, J. Phys. F. **17**, 837-848 (1987).

[23] D. Brunner, J. Diehl, Strain-Rate and temperature dependence of the tensile flow stress of high-purity α-iron above 250 K (regime i) studied by means of stress-relaxation tests, Phys. Status Solidi(a). **124**, 155-170 (1991).

[24] A. Seeger, C. Wüthrich, Dislocation relaxation processes in body-centred cubic metals, Nuovo Cim. B. **33**, 38-75 (1976).

[25] S.Z. Ke, J. Liu, F. Huang, Z. Wang, Y.J. Bi, Effect of pre-strain on hydrogen embrittlement susceptibility of DP600 steel, J. Chin. Soc. Corros. Prot. **38**, 424-430 (2018).

[26] D.P. Escobar, T. Depover, L. Duprez, K. Verbeken, M. Verhaege, Combined thermal desorption spectroscopy, differential scanning calorimetry, scanning electron microscopy and X-ray diffraction study of hydrogen trapping in cold deformed TRIP steel, Acta Mater. **60**, 2593 (2012).

[27] G.A. Young Jr, J.R. Scully, The diffusion and trapping of hydrogen in high purity aluminum, Acta Mater. **46**, 6337 (1998).